

2.B Nonlinear Evolution of Ablation Driven Rayleigh-Taylor Instability

Simulations of the Rayleigh-Taylor instability of ablatively accelerated thin-shell fusion targets show that the nonlinear evolution exhibits spike amplitude saturation due to ablative mass removal; the shell anterior surface evolves to a laminar (non-turbulent) quasi-stationary distorted state. The perturbed flow causes a significant departure from spherically symmetric behavior, but the laminar shell interior structure makes it appear possible to retain some of the advantages of larger aspect ratio fusion targets.

Spherically symmetric calculations of the behavior of laser-driven fusion targets have demonstrated major advantages of employing ablatively imploded spherical shells for obtaining optimum performance. The use of shells, as opposed to solid spheres, has been shown to reduce significantly the peak laser power required to drive successfully a target of fixed mass. In general it is predicted that performance improves with increasing shell aspect ratio, $A (\equiv r/\Delta r)$, where r and Δr are the initial radius and thickness of the shell,^{1,2,3} and the useful range of A is approximately $5 < A < 100$. Unfortunately the continuous inward acceleration of a spherical shell by ablation pressure applied to its outside surface causes an instability which is a form of the Rayleigh-Taylor instability⁴ and is capable of disrupting the spherical symmetry and subsequent thermonuclear burn enough to constitute failure. Extrapolations of linear stability theory predict failure in shells with A larger than some number near 5.^{1,3,5} To make quantitative predictions of failure, we present nonlinear ablative calculations which show important departures from the classical nonlinear development of the instability.^{6,7,8} In particular it is seen that (1) growth of the spikes tends to saturate, i.e. their growth rate decreases significantly at large amplitude and in some cases the spike structure becomes approximately stationary except for time-dependent ablative mass removal effects; (2) the spike structure resembles the classical case with an Atwood number, $\alpha = 1$,⁷ in the sense that no Kelvin-Helmholtz structure is seen;^{7,8} and (3) the flow is sufficiently distorted to cause significant departure from spherically symmetric behavior but exhibits a laminar (non-turbulent) structure. The results suggest the upper limit imposed by instability on the range of aspect ratios that can be used successfully may be extended to higher values than previously believed. Target reoptimization calculations will be required which consider the instability distortions and include the effects of converging geometry.

We study the nonlinear effects of the instability in a series of numerical simulations of a segment of a plane slab of fully ionized $Z = 6$ material accelerated between two rigid, parallel slip surfaces by ablation pressure. The ablation is driven by a constantly absorbed laser irradiance in the range $I = 2 \times 10^{14}$ to 10^{15} W/cm², deposited at a critical density of $n_e = 10^{21}$ cm⁻³.

These simulations could have been done in spherical geometry (finite A) instead of in planar geometry, ($A \rightarrow \infty$), but planar geometry avoids the choice of a particular A and makes identification of basic phenomena easier by eliminating convergence effects. The simulations were done with a two-dimensional triangular Lagrangian hydrodynamics code, DAISY, which includes nonlinear electron thermal conduction. The simulations employ 72 zones per perturbation wavelength. The resulting resolution is consistent with that required in recent Lagrangian simulations of the Rayleigh-Taylor instability of an incompressible inviscid fluid.⁷

The simulations were begun with an initially uniform shell density of 2 g/cm^3 and thickness of $3 \mu\text{m}$, and run until a quasi-steady ablative flow is established near the shell surface. At this time t_i , the simulation is made two-dimensional, and the instability is initialized by imposing a divergence-free perturbation of the form

$$\bar{\xi} = \bar{\nabla} \times (\hat{z} A_z),$$

$$A_z = (\xi_0/k_y) \sin(k_y y) \operatorname{sech} k_y(x-x_m).$$

Here x is the direction of slab motion, y runs parallel to the slab, and x_m is the point of maximum shell density. The unperturbed calculations show that the slab would be consumed by ablative mass removal at a burn-through time of about $t_b = 140 \text{ psec}$.

To determine which unstable cases are most interesting, linear instability growth rates $\gamma(k_y)$ were obtained from the planar stationary flow model of ablation^{10,11} and compared with the 2-D simulation results. In the 2-D calculation, the initialization procedure described above was used with $\xi_0/\lambda_y = 0.01$. Figure 13 shows a

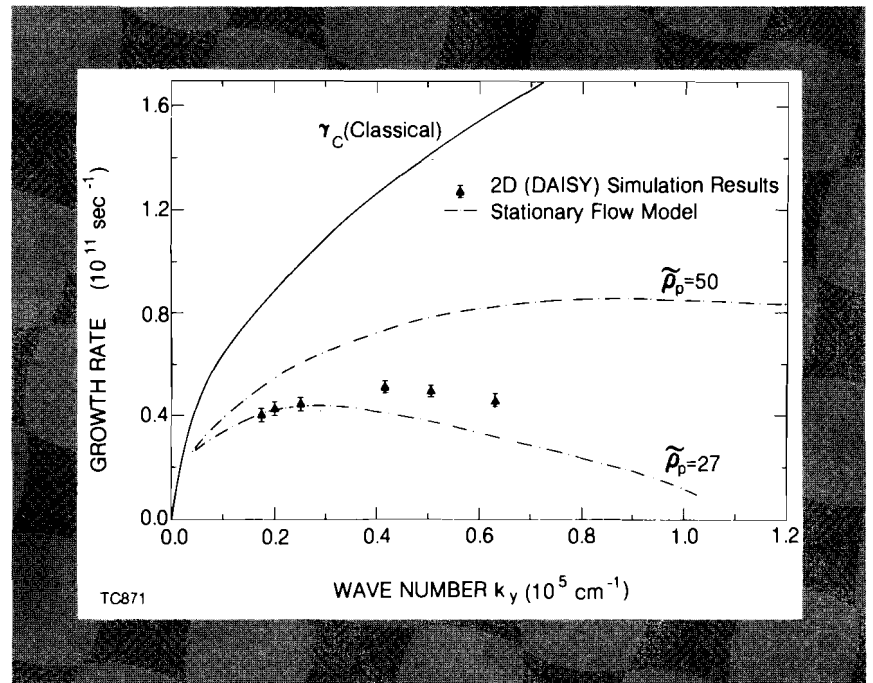


Fig. 13
Comparison of the 2D simulations of Rayleigh-Taylor linear instability growth rates with the stationary flow model.

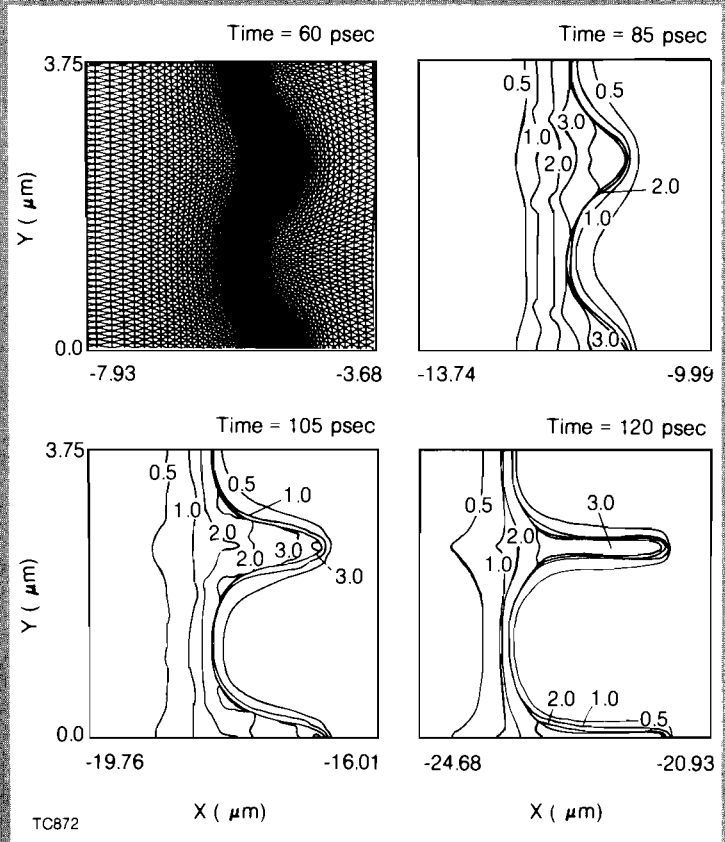


Fig. 14
Initial mesh configuration at 60 psec ($k_y \xi_0 = \pi/5$) and time evolution of the density contours for the $I = 10^{15}$ W/cm², $\lambda_y = 2.5$ μm case.

set of values of $\gamma(k_y)$ obtained with the 2-D code from an
 $I = 10^{15}$ W/cm²

zeroth order solution initialized at t_i , and $\gamma(k_y)$ obtained from the stationary model.¹¹ The stationary solutions are characterized by a single parameter, the ratio of maximum density to the isothermal sonic point density $\tilde{\rho}_p$. The simulated results are not quite stationary but correspond closely to values of $\tilde{\rho}_p \sim 27$ and are bounded by $27 \lesssim \tilde{\rho}_p \lesssim 50$ (see Fig. 13). For comparison the classical growth rates, $\gamma_c \equiv (k_y g)^{1/2}$ are shown. Ablative effects cause $\gamma(k_y)$ to reach a maximum and then decrease to zero with increasing k_y , in contrast with γ_c which increases indefinitely (Fig. 13).^{1,12} This result is consistent with previous time dependent perturbation solutions.^{1,13} The potentially troublesome and interesting range of k_y is near the maximum of $\gamma(k_y)$ and near the inverse of the shell thickness. The case $I = 10^{15}$ W/cm² and

$$k_y = 2.5 \times 10^4 \text{ cm}^{-1} (\lambda_y = 2.5 \text{ } \mu\text{m})$$

is seen from Fig.13 to be near the maximum, and was chosen, together with the

$$k_y = 6.2 \times 10^4 \text{ cm}^{-1} (\lambda_y = 1.0 \text{ } \mu\text{m})$$

case, to study the nonlinear development of the instability.

Figure 14 shows a time sequence of density contours from a run which began with the initialization shown in the first frame ($k_y \xi_o = \pi/5$). This amplitude-to-wavelength ratio is one for which linear stability analysis is valid^{7,8} initially. As the amplitude increases, structure is seen which resembles the classical Rayleigh-Taylor "bubble and spike"^{6,7,8} phenomena but unlike the classical behavior the spike does not grow indefinitely due to ablative mass removal. This is also seen in the sequence of

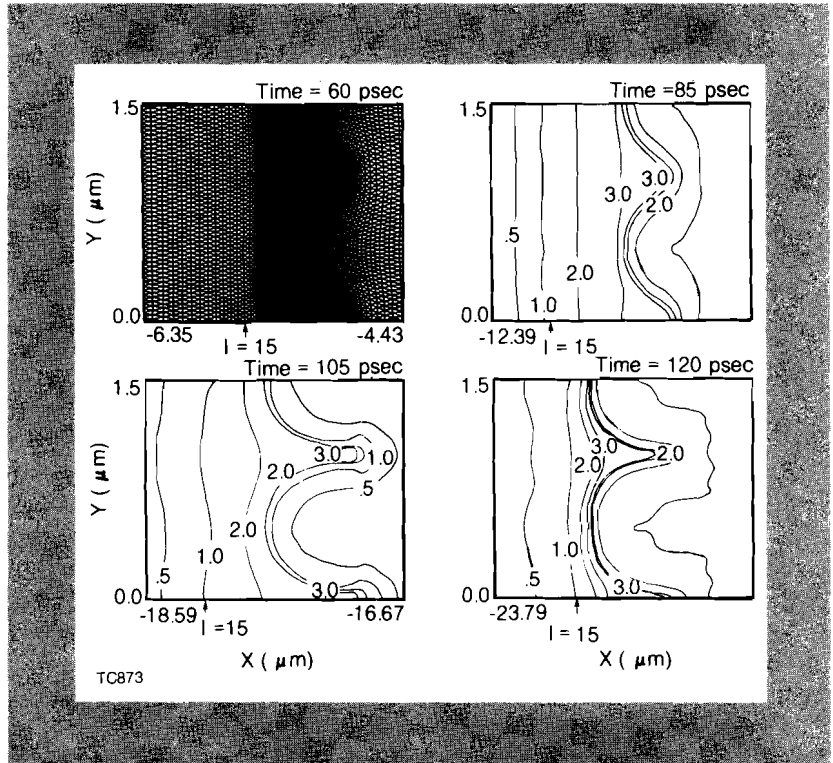


Fig. 15
Initial mesh configuration at 60 psec ($k_y \xi_o = \pi/5$) and time evolution of the density contours for the $I = 10^{15}$ W/cm², $\lambda_y = 1.0$ μm case.

contours (Fig. 15), from the 1 μm run. In Fig. 16 a superposition of $\rho = 2$ g/cm³ contours for the Fig. 15 case is shown. The $\rho = 2$ g/cm³ contour was chosen to represent the approximate position of the shell surface (ablation front) because the density gradients are largest in the neighborhood of this density. Figure 17 gives the amplitude time history of the surface distortion (defined as the separation between the bubble and the spike for the $\rho = 2$ contours). In Fig. 17 a period of exponential growth (from about 70 to 95 psec) is followed by decreased growth at an amplitude slightly less than the wavelength, followed (for the 1 μm case) by a decrease to a smaller amplitude until burn through (about 140 psec). From Fig. 16 it is seen that as the spike approaches its maximum amplitude it becomes more narrow near the tip and then broadens again as its amplitude decreases while the bottom of the bubble is seen to become progressively flatter. Figure 17 also illustrates the relative thickness of the shell at its thinnest region (top of the bubble) for the two unstable cases, together with the unperturbed ablated shell thickness. The 2.5 μm case is the most globally disruptive. From Figs. 14 and 15 it is

interesting that a quasi-stationary distorted state does not evolve into a further state of turbulent mixing.⁹ The cause of the saturated amplitude of the spike is seen to be the higher ablation pressure near the tip caused by the higher temperature there than at the same density in the bubble. Contour plots of temperature (not included) show this difference. The temperatures near the tip are larger because the tips are nearer to the heat source (the critical surface is located outside and to the right of the contour plots). Interestingly, the simulations show that the center of mass motion of the shell is virtually unchanged by the presence of the unstable Rayleigh-Taylor flow. The disruptive nature of the instability is apparent from Fig. 17. The instability evolves due to a nearly constant bubble rise velocity which removes mass from the bubble region. Particle paths from the simulations (not illustrated) indicate that the shell thickness near the bubble decreases linearly with time. The laminar nature of the flow is illustrated by the time-independent ordering of the density contours (Figs. 14 and 15).

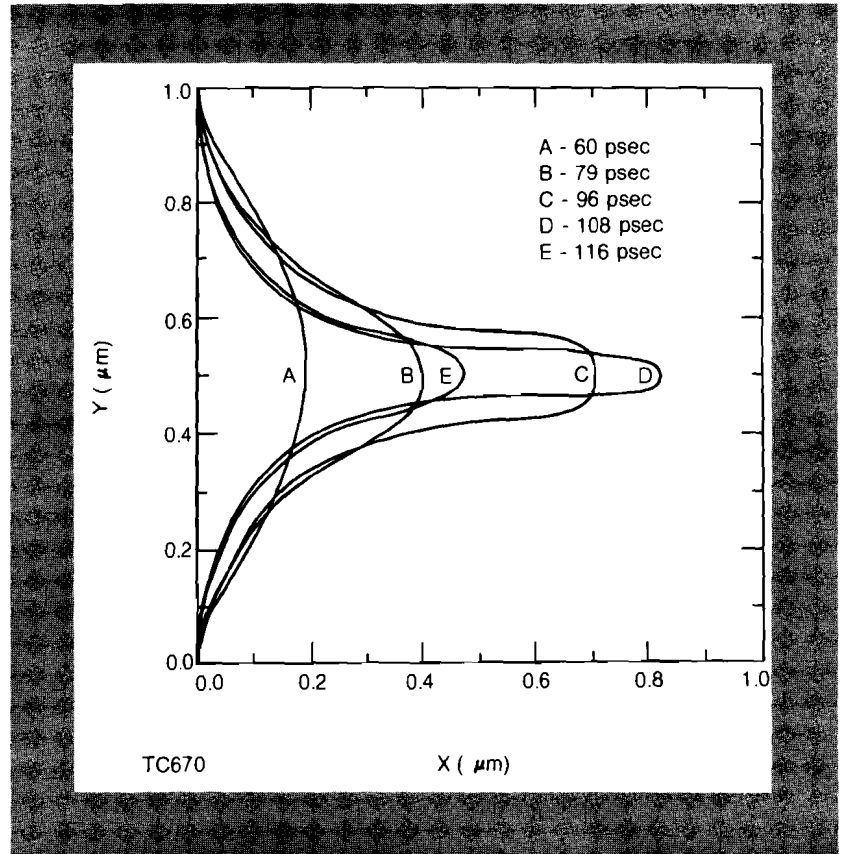
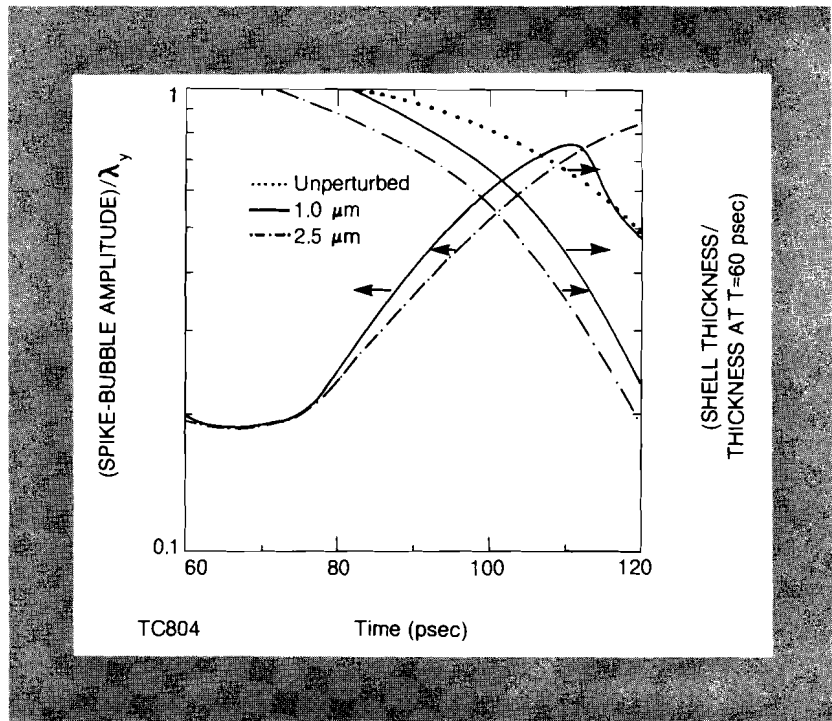


Fig. 16
Spike ($\rho = 2 \text{ g/cm}^3$ contours) at various times for the instability illustrated in Fig. 15.

We summarize by noting the form that the modes have acquired (last frames of Figs. 14 and 15) are sufficiently distorted to be a potential source of disruption of the final fuel compression of a large aspect ratio spherical fusion target. However, in both cases the left side of the shell, which is the side away from the laser and would correspond to the "inside" of a spherical shell, is seen to

Fig. 17
Spike amplitude as a function of time for the unstable cases of Figs. 14 and 15, and shell thickness at the bubble center as a function of time for the two perturbed cases compared with the unperturbed simulation.



be less distorted than the outside. This laminar and only moderately distorted inner surface, while not as desirable as a perfectly flat (or spherical) surface, would in general not be mixed with lower density fuel inside it. In Fig 15 we illustrate this effect by marking a Lagrangian surface ($l = 15$) whose position at t , corresponds to a material density near 0.8 g/cm^3 (about the density of shocked liquid D-T fuel). Consequently, somewhat better final fuel compression would be expected than if the inner surface of the shell had lost its integrity due to turbulent mixing. It therefore appears plausible that successful large aspect ratio ICF implosion systems may be designed to operate with shell distortions of the kind and amplitude seen here.

REFERENCES

1. G. Fraley, W. Gula, D. Henderson, R. McCrory, R. Malone, R. Mason and R. Morse, *Plasma Phys. and Controlled Nuc. Fusion Research*, **543**, (International Atomic Energy Agency, Vienna, Austria, 1974).
2. R.J. Mason, *Nuc. Fusion*, **15**, 1031 (1975).
3. Yu Afanas'ev et. al., *Pis'ma Zh. Eksp. Teor. Fiz.* **21**, 150 (1975) [*JETP Lett.* **21**, 68 (1975)], and *Pis'ma Zh. Eksp. Teor. Fiz.* **23**, 617 (1976) [*JETP Lett.*, **23**, 566 (1976)].
4. S. Chandrasekhar, *Hydrodynamic and Hydromagnetic Stability*, (Oxford U.P., Oxford, 1961), Chap. X.
5. R. L. McCrory and R. L. Morse, *Phys. Fluids*, **19**, 175 (1976).
6. J. D. Lindl and W. C. Mead, *Phys. Rev. Lett.* **34**, 1273 (1975).
7. G.R. Baker, D. I. Meiron and S. A. Orszag, *Phys. Fluids* **23**, 1485 (1980).